Research Article Vol. 28, No. 13 / 22 June 2020 / Optics Express 18566
Optics EXPRESS

Developing a portable gas imaging camera using highly tunable active-illumination and computer vision

KYLE J. NUTT,[1,3] NILS HEMPLER,[2] GARETH T. MAKER,[2] GRAEME P. A. MALCOLM,[2] MILES J. PADGETT,[1] AND GRAHAM M. GIBSON[1,4]

[1]SUPA, School of Physics and Astronomy, University of Glasgow, Glasgow G12 8QQ, UK
[2]M Squared Lasers Ltd, 1 Kelvin Campus, West of Scotland Science Park, Maryhill Road, Glasgow G20 0SP, UK
[3]kyle.nutt@glasgow.ac.uk
[4]graham.gibson@glasgow.ac.uk

Abstract: We have developed a portable gas imaging camera for identifying methane leaks in real-time. The camera uses active illumination from distributed feedback InGaAs laser diodes tuned to the 1653 nm methane absorption band. An InGaAs focal plane sensor array images the active illumination. The lasers are driven off resonance every alternate frame so that computer vision can extract the gas data. A colour image is captured simultaneously and the data is superimposed to guide the operator. Image stabilisation has been employed to allow detection with a moving camera, successfully imaging leaks from mains pressure gas supplies at a range of up to 3 m and flow rates as low as 0.05 L min^{-1}.

1. Background

The ability to detect and locate invisible gases is extremely desirable in a wide range of applications. For methane gas in particular there are financial, safety, legal and environmental motivators [1,2]. A device called a flame ionisation detector (FID) [3] can be used to quantify the amount of methane in a sample of air. FIDs give very accurate concentrations of methane but only at a single point so their usefulness as leak detectors is limited. In addition, the use of portable FIDs require the operator to be close to the source of the leak, sometimes placing the operator in a hazardous situation. Similar optical gas detecting technology uses the attenuation of a laser beam tuned on resonance with an absorption band of methane to detect the gas [4,5]. Such devices can be portable and work at range. However, similar to FIDs many measurements are required to locate the exact source of the gas leak. For detecting the source of a leak, exact quantities of methane are less important than being able to follow the flow of a gas cloud back to its source. Optical means of gas detection provide many avenues to gather spatial information. In this way the source of a leak can be located by using imaging techniques. Real-time gas imaging in particular allows a user to observe the flow of a gas cloud through air and thus locate its point of origin. This paper reports the design and performance of a portable gas imaging camera for gas leak detection.

Optical gas imaging uses the absorption bands of the gases to image them. This requires a source of light which emits at the absorption band of a target gas, and a detector sensitive to that light. Passive imaging systems use the optical absorption of ambient light to image a gas whereas active imaging systems use the optical absorption of laser light. There are several different techniques for extracting spatial information from the absorbed light. The spatial evolution of

#389634 https://doi.org/10.1364/OE.389634
Journal © 2020 Received 31 Jan 2020; revised 18 May 2020; accepted 22 May 2020; published 8 Jun 2020

Optics EXPRESS

the gas can be imaged directly using a focal plane array (FPA) camera. Both passive [6] and active [7] imaging systems have been demonstrated using an FPA sensor as their detector. It is also possible to use a single detector combined with a means to extract spacial information. Gas imaging systems have been demonstrated using raster scanning [8,9]. Alternatively structured illumination can be used to image methane gas with a single-pixel camera [10]. Furthermore, the field of view of an imaging system can be expanded by combining an FPA system with scanning to allow panoramic gas detection [11].

An optical gas imaging system can simply show a grey-scale image gathered by imaging on resonance with an absorption band of a target gas. This will result in a monochrome image where the target gas appears as a dark cloud [7]. Depending on the environment and the resolution of the imaging system, this gas can be difficult for a user to recognise as this information can easily be confused with other dark features in the image. Many systems instead opt to use computer vision techniques to extract the gas signal so it can be false coloured making the detected gas stand out more to a user. Furthermore, the extracted gas signal can be upsampled, correlated and overlaid onto a higher resolution image taken with a full colour camera. This makes detecting gases and locating their position in the real world very easy, even when the original gas data is of low resolution.

While there are many different methods for detecting methane, the cases where gas imaging is used in industry are still rather limited. Many gas imaging systems are bulky, difficult to use and prohibitively expensive. This means that gas imaging solutions are only employed in high value areas for infrequent monitoring, or as fixed installations. Light detection and ranging (LIDAR) based optical gas detection uses the back-scatter of laser light and time of flight measurements to image atmospheric methane over long ranges [12,13]. Such systems can be mounted on aircraft to allow the surveying of pipelines and whole industrial plants [14]. However, regular surveying work in industrial plants or in gas storage areas takes place over short range and often indoors. Thus there is potential for a gas imaging system to see mass adoption in industry if it is suitable for short-range surveying work, and more efficient and cost effective than existing techniques. With this in mind, the system needs to be easy to use and portable enough to be used by an operator without vehicular mounting in indoor and outdoor environments. The system should exploit this portability to allow work usually carried out by FIDs to be done at safer distances from potential gas leaks. With an enhancement to efficiency and safety the system will still need to be affordable enough to allow incorporation into maintenance routines.

A system could be developed using passive illumination in an attempt to save costs. However, passive illumination systems are often restricted by environmental conditions. Some require daylight, or temperature differentials between the leaking gases and their environment to operate. For a device to see widespread adoption it will need to be flexible and robust in many environments. Taking these factors into account a portable, real-time gas imaging camera was designed using active illumination.

2. Instrument design

Our gas imaging camera consists of a body which contains the flat-field active illumination with on-board electronics, a short-wave infra-red (SWIR) FPA sensor (Goldeye G-008) with a 25mm SWIR lens (Kowa LM25HC-SW), a colour webcam (Logitech c270) with a 4 mm c-mount lens, a micro-controller (Arduino Nano) for illumination modulation and a rechargeable lithium ion battery (Enix Energies MGL2806) with the necessary electronics to charge and supply power to the camera.

The entire gas imaging camera is 259 mm long, 206 mm wide, 118 mm tall, and weighs 3.2 kg. A picture of the completed gas imaging camera can be seen in Fig. 1. A single USB cable connects from a USB 3B connector to a USB 3A port on a portable laptop computer or tablet device. This portable computer handles the computer vision tasks and displays the output from

Optics EXPRESS

the processing to the end user. During development a configuration using a compact Latte Panda Alpha single-board computer and a 7 inch eDP touch display was also tested showing similar performance to that of the external computer. The Latte Panda Alpha has an integrated Arduino which can operate as the micro-controller for illumination modulation, removing the need for an additional micro-controller. Future modifications to the power supply electronics should allow full integration of the computer and display into the camera enclosure, resulting in a hand-held system.

Fig. 1. Photo of the gas imaging camera. a) Lens of the SWIR FPA detector with attached filter. b) Lens for the colour webcam. c) lens tubes containing the two active illumination modules with visible engineered diffusers.

The flat-field active illumination is provided by two Eblana Photonics EP1653-7-DM-TP39-01 InGaAs laser diodes. These diodes are designed to emit at 1653 nm and are single mode with a linewidth of less than 2 MHz. They are packaged in an industry standard TO-39 circular can and have built-in Thermo-Electric Cooling (TEC) and temperature sensor. Both diodes have been individually mounted on a circular custom circuit board which is designed to fit inside a Thorlabs 1 inch lens tube. The lens tube (Thorlabs SM1M15) and adjustable lens tube (Thorlabs SM1V05) form a compact illumination module. Two of these modules are mounted within the gas camera housing on either side of the SWIR sensor. Inside the adjustable lens tube is a f=30 mm lens which is used to collimate the output of the laser diode. The collimated laser output then passes through a 20° square engineered diffuser (Thorlabs ED1-S20-MD) which is mounted on the adjustable lens tube. The combination of the adjustable lens tube and diffuser allow the light profile from the laser diodes to be matched with the field of view of the SWIR imaging system. This ensures that the maximum possible area of the camera can image the invisible gas, while wasting as little of the illumination as possible.

Each laser diode is controlled by a Thorlabs MLD203CLN constant current LD driver chip. The built-in TEC is controlled using a similar Thorlabs MTD415T miniature PID temperature controller chip. These chips were mounted on a custom PCB to allow easy integration into the camera body. The lasers are wavelength tuned using a control voltage generated by a Data Acquisition device (DAC). The DAC used to modulate the laser current is an Analogue Devices AD5696 Quad 16bit nanoDAC+ which was mounted on a custom PCB and interfaced to the Arduino Nano. The settings on the TEC Driver were selected such that at max operating voltage

Optics EXPRESS

the laser diodes were tuned on resonance with the chosen absorption band of methane gas. Thus, if the voltage the DAC outputs is lowered the laser diodes are driven off resonance with the absorption band, with only a very minor change in overall intensity. We have found that once the TEC settings have been calibrated with corresponding on and off resonance voltage levels the system will be stable and won't need re-calibrated unless components have been changed or reseated. Simply powering up the LD and TEC controller PCB results in the laser operating at the correct drive current and temperature.

The internal camera and microcontroller connections are attached to an internal USB hub which connects to a USB 3B female port on the back of the camera body. This port allows the camera to be operated by an external Windows 10 laptop computer or tablet with installed control software written in Labview and National Instruments Vision. A schematic diagram of the gas imaging camera can be seen in Fig. 2. For applications where a standalone device is desired, the USB hub and Arduino nano & DACs can be replaced with a single-board computer and touch display, which must also be powered by the battery.

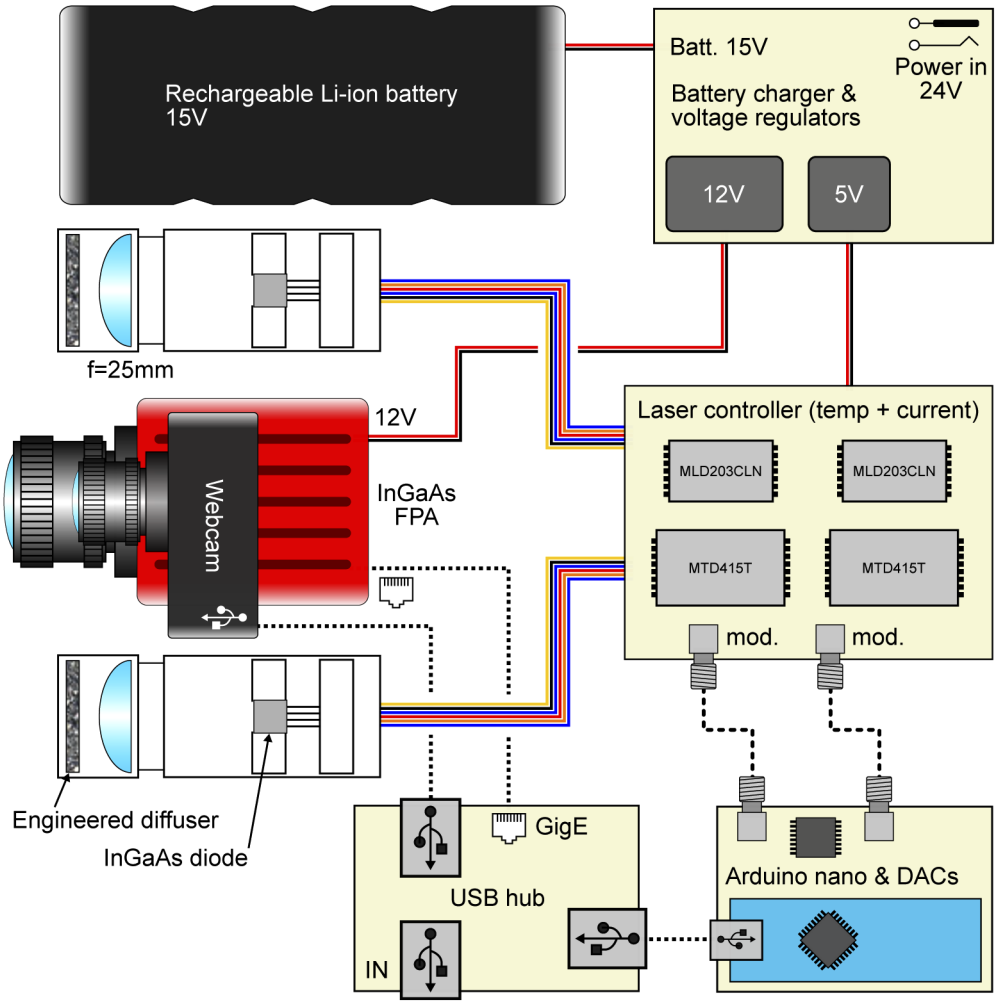

Fig. 2. Schematic diagram showing the hardware design of the gas imaging camera

Optics EXPRESS

3. Laboratory characterisation

Methane has a Lower Explosive Limit (LEL) of 5 % concentration in air. Many early warning detectors will list their sensitivity as percentage of LEL, as detecting the presence of methane gas in a closed environment before the concentration reaches the LEL is desired. However, this metric is less useful when attempting to locate the source of a pure methane gas leak. Kitchen hobs excrete nearly pure methane gas, but household detectors are recommended to be placed near the ceiling and a metre or two displaced from directly above the hobs. This is because a high concentration methane cloud can rise from a kitchen hob before ignition, but will quickly dissipate. If these sorts of emissions triggered household gas detectors users would interpret these alarms as false positives. With the gas detector placed further away and near the ceiling it will detect a steady build up within the room.

In the case of a gas leak, gas will start out nearly pure and then dissipate through the air and around obstacles as it rises or is affected by air currents. Thus while LEL is a valuable metric in the previous case, a different metric is more applicable to our gas imaging camera. The sensitivity of the gas imaging camera was tested using gas cells containing pure methane gas. This allows the sensitivity of the gas camera to be measured in relative thickness of pure methane gas. A 100 mm methane cloud of 10 % concentration is equivalent to a 10 mm methane cloud of 100 % concentration. The gas cells used had an internal cavity of width 68 mm, height 44 mm and thicknesses varying from (2.47±0.02) mm, (4.70±0.05) mm and (9.4±0.1) mm. The active illumination travels first through the glass cell and then back-scatters off of the scene before passing through the glass cell again. However to keep the metric intuitive, width of relative pure methane will be used instead of optical path length through methane. The gas cells were placed against black card and imaged at various distances with 50 ms and 33.3 ms exposures. The gas cells positioned against the black card can be seen in Fig. 3 with the detected gas information superimposed on top. The black card appears as a medium grey in the SWIR. The gas imaging camera was able to detect all the gas cells that contained methane at a range of up to 3 m.

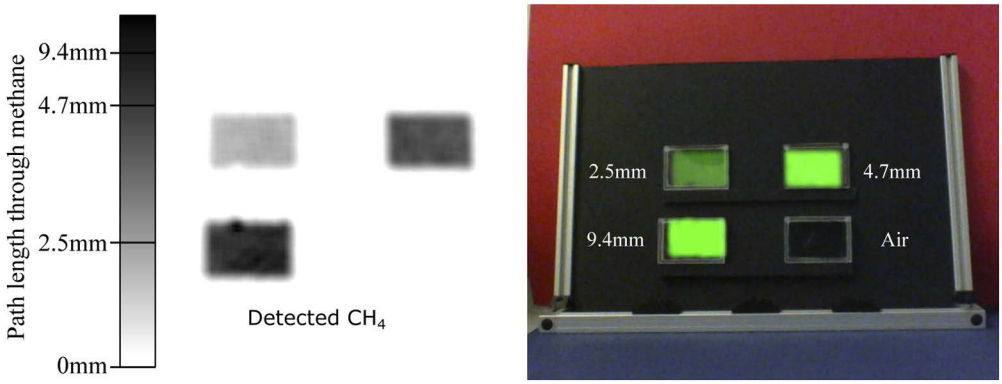

Fig. 3. *Left:* The result of an image subtraction of on and off resonance SWIR images with post filtering. Scaled for visibility. Darker areas correspond to greater path length through methane. *Right:* The result of the SWIR image subtraction applied over a full colour image of the scene. Greener areas correspond to greater path length through methane.

The results show how the transparency of the green layer corresponds to the relative path distance through pure methane. Thin or dilute gas clouds appear fainter than those that are thick or concentrated. In addition, the contrast of the gas signal also depends on the material properties of the back-scatter surface, viewing angle and ambient light levels. This presents challenges for calibrating the camera for the accurate measurement of gas concentration or flow rate that is required for applications beyond leak detection. However, the software allows the operator to

Optics EXPRESS

locate the source of a gas leak by scaling the detected signal so that it is clearly visible against the background.

The gas imaging camera was then used to image controlled gas emissions at mains household pressure of (20±2) mbar from a standard gas line copper pipe. A manometer allowed the measurement of the pressure inside the copper pipe in mm H_2O. A pressure reading of 203.9 mm H_2O on the manometer corresponds to the household pressure of 20 mbar. A gas leak was simulated by intentionally loosening one nut on a T-junction connector. By using a flow regulator and a wrench on the T-junction the system could be set to leak at specific flow

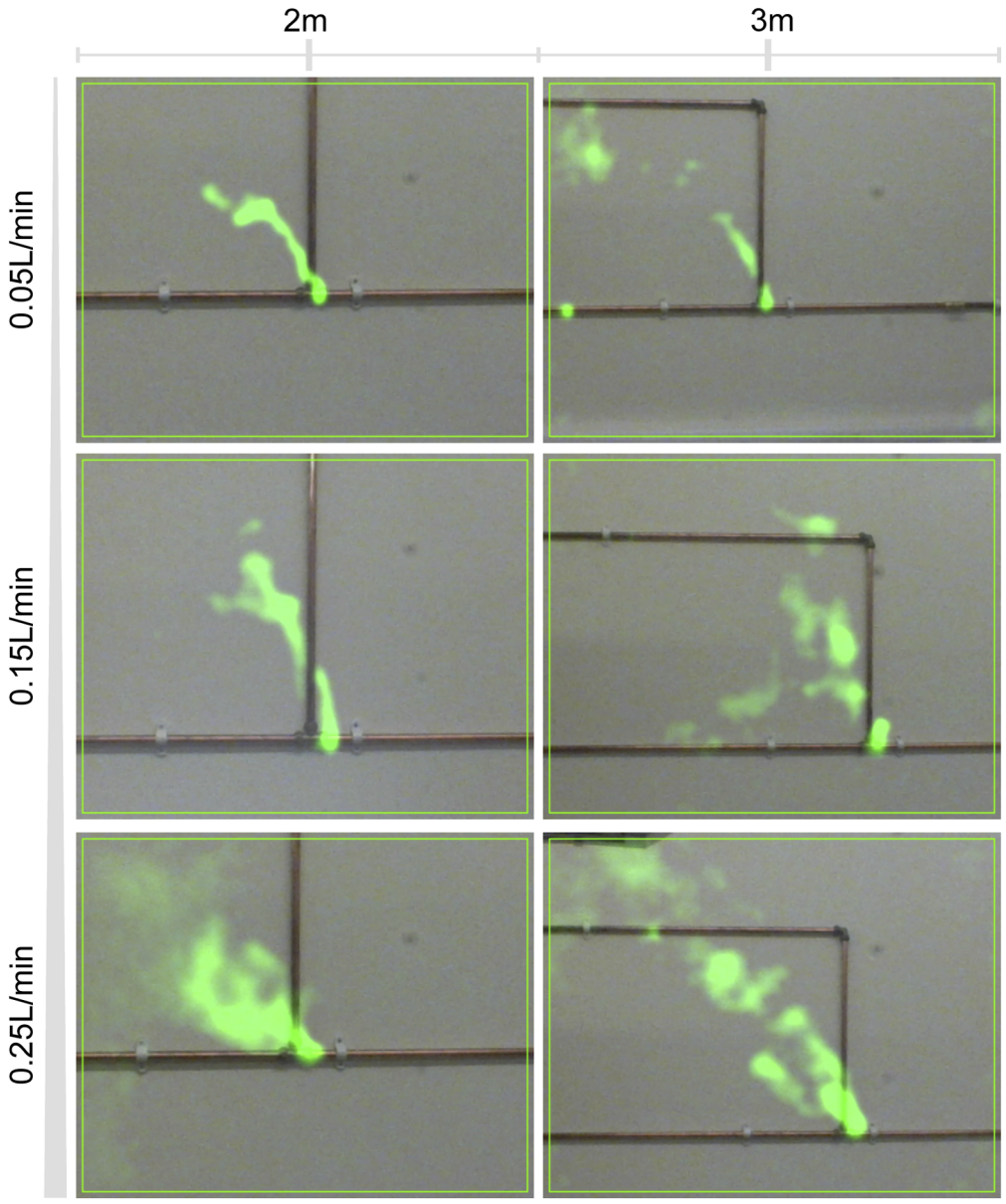

Fig. 4. Images extracted from 10 Hz test videos at a range of 2 m and 3 m, and at flow rates of 0.05 L min^{-1}, 0.15 L min^{-1} and 0.25 L min^{-1}

Optics EXPRESS

rates with a set pressure. The selected flow rates were 0.05 L min^{-1}, 0.15 L min^{-1}, 0.25 L min^{-1} and 0.35 L min^{-1}. A gas plume was released at each of these flow rates with a fixed household pressure. Each of the resulting gas plumes were imaged at a range of 1 m, 2 m and 3 m. At each range the gas imaging camera was refocused. This was achieved by temporarily switching to the unprocessed SWIR images. Whilst having a sharp focus is not strictly necessary, a softer focus results in a lower contrast in the gas signal, reducing the sensitivity. This is particularly the case when imaging smaller leaks. Refocusing should take place when the range of imaging changes by 0.3 m to 0.5 m to maintain reliability in detection of narrow gas plumes.

At each range gas was visible and motion could be tracked, allowing the source of the leak to be located. Each gas plume originates at the T-junction in a high purity stream which appears clearly in the live image feed. This high purity stream begins to mix with air and follows the surrounding air currents. As the resulting gas-cloud becomes more mixed its colour fades on the live image feed. For higher flow rates, the cloud remains high purity for longer and thus appears as a stronger colour. However, even small leaks were visible from range. The methane appears to cluster together as it moves causing puffs of methane to be visible similar distances from the source as for the high flow rates. As the detection range increased and the flow rates lowered it was necessary to increase a scaling factor for viewing the gas signal. It is likely that higher air currents would also necessitate increasing this scaling factor as the methane gas would dissipate faster. In the images shown in Fig. 4, a constant draft can be seen moving the gas cloud from the right side of the scene to the left. This draft was not intentionally created or controlled, it is an effect caused by the ventilation inside the lab space.

There were other uncontrolled factors discovered through testing which effected the formation of gas clouds. If the room was rapidly cooled with air conditioning such that the methane gas was warmer than the surrounding air, the gas would float rapidly in an almost vertical column and would not appear cloud-like. Conversely if the room was rapidly heated then the gas would have more time to dissipate before rising, and may even initially sink below the source. For the images in this paper the methane and the air were at thermal equilibrium, where the gas rises mainly due to its density compared to the surrounding air.

4. Application and evaluation

For real world applications the gas imaging camera will be operated either tripod mounted or hand-held with the use of a shoulder mount. In this paper the functionality of the gas imaging camera is demonstrated with an external laptop computer attached by USB cable. However, there is capacity within the existing camera housing for an on-board computer and integrated touch display to allow the camera to be completely stand-alone. In either configuration, when an operator is using the camera, movement of camera location between on and off resonance images is likely. Image subtraction is a simple movement detection algorithm which will detect this motion. Camera movement between subsequent exposures will result in artefacts such as edge enhancement. These artefacts can be minimised by attempting to re-align the consecutive frames before performing an image subtraction. There are many algorithms for aligning features in two images, however most are unsuited to real-time applications or don't preserve image pixel values. Phase correlation is a suitably fast algorithm which uses frequency domain analysis to align two images based on their spectral information without changing pixel values or warping features. Phase correlation requires a scene to have sufficient characteristic frequency components for the alignment to be successful. These features don't need to be excessively sharp, and refocusing every 0.3 m to 0.5 m will be sufficient to maintain stabilisation. Phase correlation cannot account for when objects rotate, change size or shift proportions due to perspective changes. Therefore, the operator needs to be mindful of how they handle and move the camera. For example, excessive rotational movement of the camera should be avoided while searching for leaks. Also, it should not be positioned in a way where nearby objects obscure parts of the scene, especially during

Optics EXPRESS

lateral motion. Lastly, moving objects within the scene, or those exhibiting vibrational motion, may result in artefacts that cannot be suppressed by phase correlation. However, the colour video feed helps the operator to mitigate such issues.

Phase correlation is applied to consecutive frames from the InGaAs camera to calculate the translation necessary to move the frames back into alignment if movement is detected. Image transforms and sub-pixel interpolation is not applied so re-alignment will only ever be to the nearest pixel. Blurring algorithms are used to remove remaining narrow edge structures while preserving gas data. However, the active illumination also moves with the camera, so when consecutive frames are correlated, the light source has changed relative location. Moving light sources cause shadows to change location, which can also create false positives. Furthermore, the light profile is shaped to be as flat as possible, but there is still a light intensity gradient. In particular, the light gradient is steep enough at the edges of the illumination pattern to create a noticeable differential when camera movement occurs. This issue was extremely pronounced before the addition of the engineered diffusers. Initially the output of each laser diode was expanded to fill the field of view of the camera, resulting in a Gaussian shaped profile illumination of the scene rather than the flat profile illumination desired. The addition of engineered diffusers flatten the illumination profile and greatly reduce this effect, as can be seen in Fig. 5. However, due to the illumination from each laser not overlapping perfectly at the edges of the scene, this effect is not completely removed and can be further compounded by the vignetting of the camera lens. Thus a further step is required to remove the false positives created by the light profile enhancement.

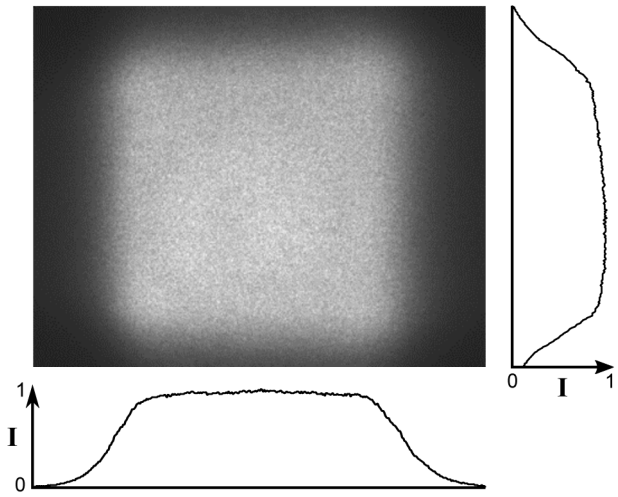

Fig. 5. Image of the light profile created with one of the laser diodes passing through an engineered optical diffuser, beside the normalised average intensity in the rows and columns. Under normal operation two lasers are used in conjunction to cover the whole field of view of the camera, overlapping in the centre.

The lasers are modulated on and off resonance each consecutive exposure of the SWIR image feed. This means that two image subtractions are carried out for each single frame of on resonance gas cloud. In the cases where the camera is moving in the same direction, the light profile enhancements are on opposite sides of the image in each subtraction, but the gas signal remains static. Thus, a binary mask can be created of both images which includes the gas signal and the light profile. Doing a logic AND operation between these two binary masks removes the shifted false positives while preserving the static gas signal. It was found that this algorithm allows gas to be imaged over the complete field of view of the SWIR imaging system.

Optics EXPRESS

With these factors taken into consideration, the camera can then be used to image methane gas leaks with a non-stationary camera. False positives may still occur if parallax effects cause objects to move within the scene, or if the camera rotates significantly. An operator can pan, tilt, truck and pedestal the camera without obscuring the gas signal. Due to the assumptions made in the AND operation, if the camera changes direction or speed of movement rapidly between frames, light profile enhancements can still occur at the edge of an output image. These effects last for a single frame until movement normalises. This was demonstrated by mounting the camera on a tripod and panning and tilting the camera, as well as pedestal and trucking the camera by hand. The image stabilisation algorithm proved suitably stable so long as there were enough features within the frame to allow correlation. This means the algorithm would be less effective in featureless environments, or in those with periodic features.

Thus, the final algorithm captures three SWIR images, alternating between on and off resonance of the target gas. Phase correlation aligns the features in each image and then two different image subtractions are performed on sequential frames. A threshold is applied to both subtractions to make binary masks, and an AND operation is performed between them. The resulting mask allows the gas image to be extracted and superimposed onto a full colour image captured simultaneously with the final SWIR image. Then, a new SWIR and colour image are captured and the process is repeated. Parallel computing allows this algorithm to execute at a rate of 10Hz.

For a demonstration of a real world use case, copper gas pipes were filled with methane gas and kept at household pressure. One of the pipe junctions was then loosened so the seal was faulty. The images in Fig. 6 shows a gas leak of 0.35 L min^{-1} being imaged at a range of 2 m

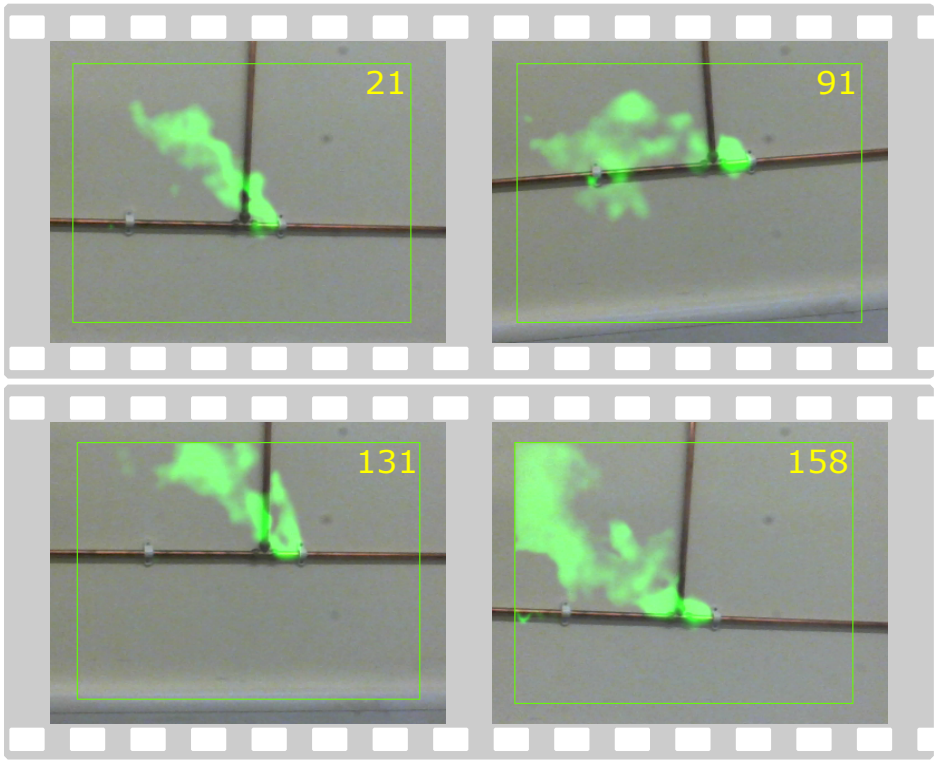

Fig. 6. Images extracted from 10 Hz test videos of a leaking pipe at 20 mbar pressure at a range of 2 m. The yellow number super-imposed on the frame is the number of the frame in the supplementary video (see Visualization 1).

Optics EXPRESS

with the camera mounted on a tripod and being panned across the length of the pipe. Each of the images are numbered to show their relative location in a 160 frame, 10 Hz, video. In these images minor movement effects are still visible, however the gas leak is still clear and visible. Minor false positives can be seen along the copper pipe. This is due to the reflective surface of the pipe causing light level fluctuations. This can be seen in the supplementary video (see Visualization 1).

The backscatter surfaces used in this work are mainly black card and light painted plasterboard wall. Surfaces having a high absorption in the SWIR will provide a poor contrast for gas imaging. Therefore, an important consideration when using the gas camera in an industrial setting is the material properties of the backgrounds likely to be encountered (a useful table showing reflectance values for a range of targets is provided by Iseki et al. [4]). We have successfully imaged gas indoors against other background materials including, dark fabric, foam sheeting and exposed brickwork. With the functionality and viability of the technique demonstrated in this work, future studies will involve a direct comparison with an industry standard device in an industrial setting. Further development of the camera to a self contained, hand-held, configuration will facilitate this work. Also, the development of an algorithm to suppress unusually large light fluctuations could remove false positives created by highly reflective metal surfaces such as pipes, and higher power lasers could offer greater sensitivity by decreasing the edge enhancement issues discussed above.

5. Conclusion

We have demonstrated portable methane imaging in real-time at a rate of 10 Hz using InGaAs distributed feedback laser diodes and a commercial InGaAs FPA sensor. Our device utilises an image stabilisation algorithm to be resilient to operator movement and displays imaged methane gas correlated over a full colour scene using computer vision techniques. This allows straightforward gas detection and location. Further improvements could be made to the device hardware by using more powerful lasers, provided the output is still eye safe, and using a more sensitive camera with less noise. The device software could be improved using optimisation techniques to increase the frame rate of the camera or allowing more sophisticated algorithms to be implemented at the current frame rate. Advances in computer hardware will also allow improvements in performance or a reduction in cost over time.

Our gas imaging camera has potential to be developed into a tool in industry for surveying work or for leak location in emergency situations. Furthermore, it has potential as an academic tool for exploring how invisible gases behave in various conditions through direct observation.

Funding

Engineering and Physical Sciences Research Council (EP/M01326X/1).

Disclosures

N.H, G.T.M and G.P.A.M are employees of M-squared lasers, an equipment manufacturer, that has a commercial interest in this work and may further develop the system for commercial exploitation.

Data availability

The data used to produce the content of this manuscript is available at http://dx.doi.org/10.5525/gla.researchdata.1013.

Optics EXPRESS

References

1. E. Naranjo, S. Baliga, and P. Bernascolle, "IR gas imaging in an industrial setting," in *Thermosense XXXII* vol. 7661 R. B. Dinwiddie and M. Safai, eds. (SPIE, 2010), p. 76610K.
2. M. Gålfalk, G. Olofsson, P. Crill, and D. Bastviken, "Making methane visible," Nat. Clim. Change **6**(4), 426–430 (2016).
3. C. F. Simpson and T. A. Gough, "Direct quantitative analysis using flame ionisation detection. The construction and performance of the FIDOH detector," J. Chromatogr. Sci. **19**(6), 275–282 (1981).
4. T. Iseki, H. Tai, and K. Kimura, "A portable remote methane sensor using a tunable diode laser," Meas. Sci. Technol. **11**(6), 594–602 (2000).
5. B. van Well, S. Murray, J. Hodgkinson, R. Pride, R. Strzoda, G. Gibson, and M. Padgett, "An open-path, hand-held laser system for the detection of methane gas," J. Opt. A: Pure Appl. Opt. **7**(6), S420–S424 (2005).
6. B. R. Cosofret, W. J. Marinelli, T. Ustun, C. M. Gittins, M. T. Boies, M. F. Hinds, D. C. Rossi, R. Coxe, S. Chang, B. D. Green, and T. Nakamura, "Passive infrared imaging sensor for standoff detection of methane leaks," in *Chemical and Biological Standoff Detection II*, vol. 5584 J. O. Jensen and J.-M. Thériault, eds. (SPIE, 2004), pp. 93–99.
7. T. J. Kulp, P. Powers, R. Kennedy, and U.-B. Goers, "Development of a pulsed backscatter-absorption gas-imaging system and its application to the visualization of natural gas leaks," Appl. Opt. **37**(18), 3912–3922 (1998).
8. G. Gibson, B. van Well, J. Hodgkinson, R. Pride, R. Strzoda, S. Murray, S. Bishton, and M. Padgett, "Imaging of methane gas using a scanning, open-path laser system," New J. Phys. **8**(2), 26 (2006).
9. D. Stothard, M. Dunn, and C. Rae, "Hyperspectral imaging of gases with a continuous-wave pump-enhanced optical parametric oscillator," Opt. Express **12**(5), 947–955 (2004).
10. G. M. Gibson, B. Sun, M. P. Edgar, D. B. Phillips, N. Hempler, G. T. Maker, G. P. A. Malcolm, and M. J. Padgett, "Real-time imaging of methane gas leaks using a single-pixel camera," Opt. Express **25**(4), 2998–3005 (2017).
11. G. Matz, P. Rusch, H.-H. Gerhard, J.-H. Gerhard, and R. H. Volker Schlabs, "New scanning infrared gas imaging system (SIGIS 2) for emergency response forces," in *Chemical and Biological Standoff Detection III*, vol. 5995 J. O. Jensen and J.-M. Thériault, eds. (SPIE, 2005), p. 59950J.
12. N. S. Prasad and A. R. Geiger, "Remote sensing of propane and methane by means of a differential absorption lidar by topographic reflection," Opt. Eng. **35**(4), 1105–1111 (1996).
13. K. Ikuta, N. Yoshikane, N. Vasa, Y. Oki, M. Maeda, M. Uchiumi, Y. Tsumura, J. Nakagawa, and N. Kawada, "Differential absorption lidar at 1.67 μm for remote sensing of methane leakage," Jpn. J. Appl. Phys. **38**(Part 1, No. 1A), 110–114 (1999).
14. J. Bartholomew, P. Lyman, C. Weimer, and W. Tandy, "Wide area methane emissions mapping with airborne IPDA lidar," in *Lidar Remote Sensing for Environmental Monitoring 2017*, vol. 10406 U. N. Singh, ed. (SPIE, 2017), p. 1040607.